ACS APPLIED MATERIALS & INTERFACES

Research Article

www.acsami.org

Charge Transport in Light Emitting Devices Based on Colloidal Quantum Dots and a Solution-Processed Nickel Oxide Layer

Huu Tuan Nguyen,[§] Huiseong Jeong, Ji-Yong Park, Y. H. Ahn, and Soonil Lee*

Department of Energy Systems Research, Ajou University, Suwon, Gyeonggi-do 443−749, Republic of Korea

Supporting Information

ABSTRACT: We fabricated hybrid light emitting devices based on colloidal CdSe/ZnS core/shell quantum dots and a solution-processed NiO layer. The use of a sol−gel NiO layer as a hole injection layer (HIL) resulted in overall improvement in device operation compared to a control device with a more conventional poly(3,4-ethylenedioxythiophene):poly(styrenesulfonate) HIL. In particular, luminous efficiency increased substantially because of the suppression of excessive currents and became as large as 2.45 cd/A. To manifest the origin of current reduction, temperature- and electric field-dependent variations of currents with respect to bias voltages were investigated. In a low bias voltage range below the threshold for luminance turn-on, the Poole−Frenkel (PF) emission mechanism was responsible for the current−density variation. However, the space-charge-limited current modified with PF-type mobility ruled the current−density variation in high bias voltage range above the threshold.

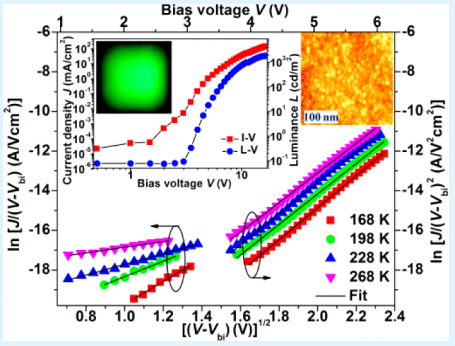

KEYWORDS: *CdSe/ZnS quantum-dot LED, nickel oxide, Poole−Frenkel emission mechanism, space charge limited current, Poole−Frenkel mobility*

INTRODUCTION

Recently, nickel oxide (NiO) thin films have been widely used as a p-type material in organic light emitting devices (OLEDs) and quantum dot (QD) based light emitting devices (QLEDs) because they are easy to form and have good physical properties.[1−9] Typically, NiO thin films were deposited by using vacuum techniques. For example, Chan et al. fabricated OLEDs with a sputter-deposited thin NiO layer.[1,2] Insertion of a NiO layer between an indium tin oxide (ITO) anode and an organic hole transport layer (HTL) in their devices with an emitting layer (EML) of tris-(8-hydroxyquinoline)aluminum (Alq_3) resulted in current−density and luminance increases. Compared to control devices without a NiO layer, current density increased from 450 to 650 mA/cm^2, and luminance increased from 8000 to 10000 cd/m^2. Another example of Alq_3 devices with a vacuum-process NiO was reported by Im et al.[3] They formed a NiO layer by combining thermal evaporation with subsequent oxidation at 500 °C. Their devices showed a significant improvement in device performance and the luminous efficiency as large as 2.7 cd/A. One of the first examples of QLEDs with a NiO layer was reported by Caruge et al.[4] However, the maximum quantum efficiency and luminous yield of their red-emitting CdSe/ZnS−QD device with a sputter-deposited NiO layer were only 0.18% and ∼1 cd/A, respectively.

Metal-organic chemical vapor deposition (MOCVD) is an advanced technique to deposit high-quality NiO layers that are appropriate for electronic devices because of a large band gap and a high permittivity.[5−9] Epitaxial NiO layers on AlGaN/GaN heterostructures, the conduction mechanism of which Fiorenza et al. studied, are an example of high-quality NiO layers. They showed that the current conduction through such a NiO layer was ruled by a Poole−Frenkel (PF) emission mechanism and that there were preferential current spots that were associated with the defects responsible for PF emission.[10]

In this work, a p-type NiO layer was deposited by using a two-step process that consisted of spin-coating of a precursor solution and subsequent thermal annealing[11] to form a hole injection layer (HIL) for green-emitting QLEDs based on CdSe/ZnS QDs. Colloidal core/shell QDs are promising EML materials because they cover a large spectral range with high color purity and good luminous efficiency.[12−18] However, the formation of a uniform QD layer is not easy. To alleviate this difficulty, a layer of poly-(*N*,*N*′-bis(4-butylphenyl)-*N*,*N*′-bis-(phenyl)benzidine) (poly-TPD) that had facilitated the formation of a neat QD EML[19] was deposited onto a sol−gel NiO layer. The use of a poly-TPD HTL in combination with a poly(3,4-ethylenedioxythiophene):poly(styrenesulfonate) (PEDOT:PSS) HIL is common in OLEDs and QLEDs. In our previous study on CdSe/ZnS QLEDs, the combination of a PEDOT:PSS HIL and a poly-TPD HTL resulted in hole-dominant devices.[19] However, the substitution of a solution-processed NiO layer for a PEDOT:PSS HIL induced a substantial change in QLED operation. To elucidate the origin of a large change in luminous efficiency, we investigated the temperature dependence of current density−voltage (J−V)

Received: January 27, 2014
Accepted: April 21, 2014
Published: May 7, 2014

characteristics. In particular, we studied temperature- and electric field-dependent current−density variations in reference to models such as the PF emission mechanism and the space-charge-limited current (SCLC) model modified with a PF-type mobility.[20−22]

RESULTS AND DISCUSSION

Figure 1 shows the comparison of the variations in current density (J) and luminance (L) with respect to the bias voltage

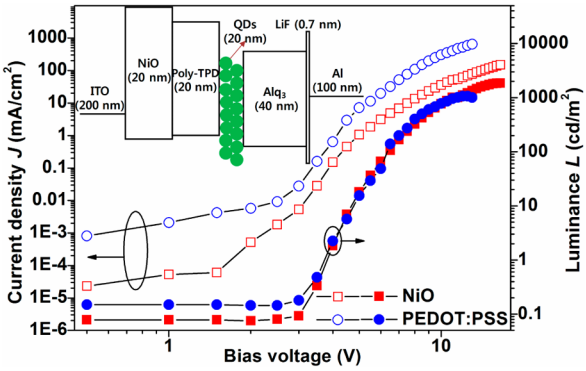

Figure 1. Variations of current density and luminance with respect to bias voltage at room temperature. Inset is an energy-level diagram for QLEDs with a NiO hole-injection layer, showing electron affinity, ionization energy, and/or work function of each layer. In the case of control devices, a NiO layer is substituted with a PEDOT:PSS layer.

(V) between two QLED devices having either a NiO or a PEDOT:PSS HIL, the thickness of which is 20 nm. Both the current−density and luminance variations are large in high-bias ranges, whereas those in low-bias ranges are small. One distinctive feature is the difference between the J−V and L−V curves. The L−V curves show almost identical turn-on threshold of ∼3 V and similar luminance levels at above-threshold voltages up to 12 V for both types of devices. However, the J−V curves show that the current of the PEDOT:PSS device is about an order of magnitude larger than that of the NiO device in the same bias voltage range. The luminance of the NiO device is as large as 1850 cd/m^2 at the bias voltage of 16.5 V.

Figure 2 shows typical EL spectra measured at 10 V, the luminance of which are 765 and 780 cd/m^2 for the NiO and PEDOT:PSS devices, respectively. We note that there is no apparent features corresponding to Alq_3 emission in the normalized EL spectra of both devices. Compared to a PL peak in the inset, the PEDOT:PSS device's EL peak is red-shifted by 20 nm and broader by 4 nm in fwhm (full width at half-maximum). However, the EL peak of the NiO device at 549 nm, the fwhm of which is 37 nm, is narrower than the PL peak by 5 nm and red-shifted only by 12 nm. Such a narrow green EL peak results in good color purity with the CIE color coordinates of (0.17, 0.74). Moreover, sharp EL spectra without any Alq_3-emission contamination indicates that electron-hole recombination in CdSe/ZnS−QD layers is responsible for the measured luminance for both types of devices.

Similar luminance at lower current density results in higher device efficiency for the NiO device as shown in Figure 3. The luminous efficiency of the NiO device that is as large as 2.43−2.28 cd/A in the luminance range of 170−1000 cd/m^2 is 6−8 times larger than that of the PEDOT:PSS device. Similarly, the power efficiency of ∼0.4 lm/W of the NiO device at the

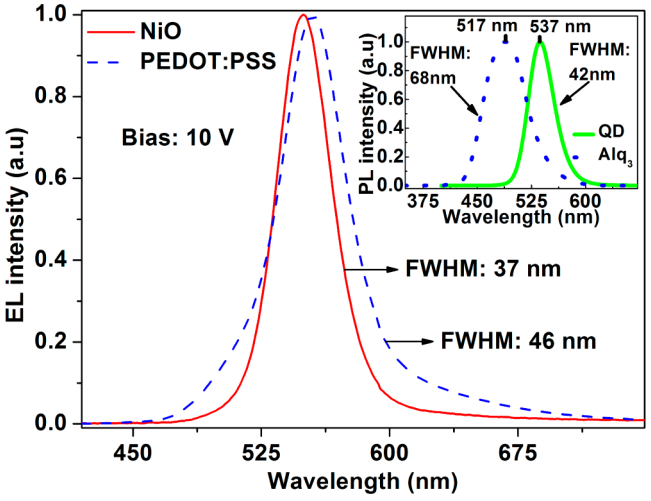

Figure 2. Normalized EL spectra of the QLEDs with either a NiO or a PEDOT:PSS hole-injection layer. The position and fwhm of NiO-device's EL peak are 549 and 37 nm, whereas those for the PEDOT:PSS device are 555 and 46 nm. The inset shows the PL spectra of CdSe/ZnS−QD and Alq_3 films. The peak position and fwhm of CdSe/ZnS QDs are 537 and 42 nm, respectively.

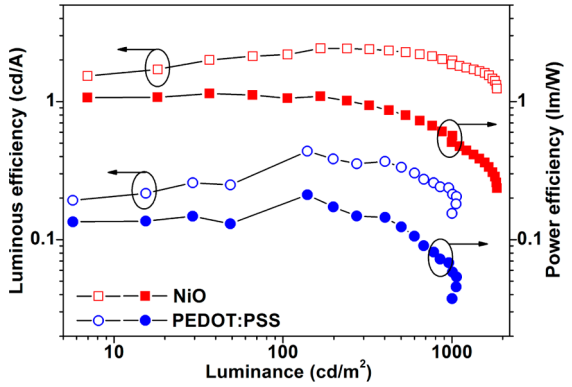

Figure 3. Comparison of luminous and power efficiencies between the QLEDs with a NiO or a PEDOT:PSS HIL. Both efficiencies were estimated from the J−V curves in Figure 1.

luminance of hundreds of cd/m^2 is 5−6 times larger than that of the PEDOT:PSS device. The maximum QE of 0.86% of the NiO device is about 3.4 times larger than that of the PEDOT:PSS device as well (data not shown). Moreover, NiO-device's QE exceeds 0.5% up to current−density of 120 mA/cm^2 and is significantly larger than those of other recently reported QLEDs that used NiO as a p-type charge transport layer.[4,11,23]

We attribute the higher efficiency of the NiO device to the suppression of excessive hole currents. The energy-level diagram in the inset of Figure 1 indicates that both types of QLEDs are hole-dominant devices as previously reported.[19,23] Hole currents start to flow first at low bias voltages and remain as a dominant component throughout the operation to a high bias voltage range. On the contrary, noticeable injection of electrons coincides with the luminance turn-on, and moreover, similar luminance values indicate that electron currents in these two devices are similar at above-threshold voltages.

To elucidate the origin of hole-current suppression in the NiO device, we examined temperature-dependent variations of currents with respect to bias voltages. Figure 4 shows a series of

dx.doi.org/10.1021/am500593a | ACS Appl. Mater. Interfaces 2014, 6, 7286−7291

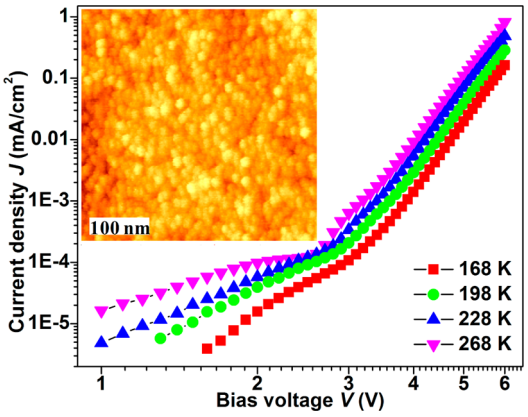

Figure 4. Variations of current density with respect to bias voltage of the NiO device at different temperatures. The inset shows an AFM image of a NiO film on an ITO substrate.

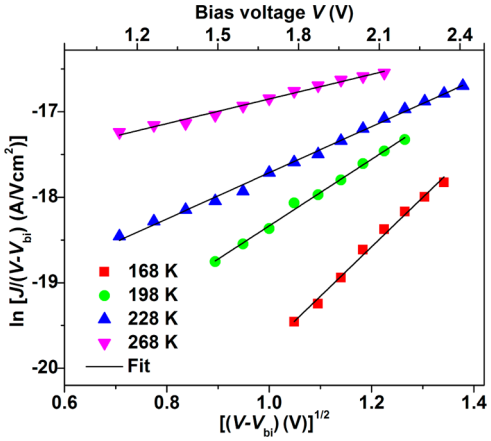

Figure 5. Poole–Frenkel emission plots, ln $J/(V - V_{bi})$ versus $(V - V_{bi})^{1/2}$, of the current variations with respect to bias voltage at different temperatures. These plots correspond to the J–V curves of the NiO device (see Figure 4) in a low bias voltage range below the threshold for luminance turn-on.

J–V curves of the NiO device measured at temperatures of 268, 228, 198, and 168 K. The log–log J–V plots show two distinctive regions corresponding to different temperature dependence. Above the threshold bias of ∼3 V for luminance turn-on, all the J–V curves in log–log scale show a similar slope. However, there is a significant slope variation below the threshold bias, from 1.7 to 5.2 (log A)·(log V)$^{-1}$ corresponding to the temperature decrease from 268 to 168 K. Such large temperature dependence indicates that a thermal activation process must be responsible for the hole-only currents below the threshold bias.

A systematic study has shown that the PF emission mechanism that refers to electric-field-enhanced thermal emission of charge carriers from Coulombic traps into a bulk band[10,20,21] is appropriate to account for the variations of hole-only currents in subthreshold bias voltage range. According to the PF emission mechanism, the current density that depends on both temperature and electric field is given as

$$J = CE_{NiO}\exp\left[\frac{-q(\varphi_t^{NiO} - \sqrt{qE_{NiO}/\pi\varepsilon_0\varepsilon_{NiO}})}{kT}\right] \quad (1)$$

where E_{NiO} is the electric field in the NiO layer, q is the electron charge, ϕ_t^{NiO} is the barrier height for charge-carrier emission from the trap states, ε_{NiO} is the relative dielectric permittivity of a NiO layer, ε_0 is the permittivity of free space, T is absolute temperature, and k is Boltzmann's constant. Within a rigid-band model, E_{NiO} is proportional to the corrected bias voltage $(V - V_{bi})$ that takes into account a built-in potential V_{bi}, the value of which is estimated to be 0.5 V from the difference between the work functions of the ITO anode (4.8 eV) and the Al cathode (4.3 eV).[24,25] Integration of the electric field inside the NiO device that consists of four layers having thickness d_i and relative dielectric permittivity ε_i (i = NiO, Poly-TPD, QD, or Alq_3) must be equivalent to the corrected bias voltage under appropriate boundary conditions. For example, if there are no interfacial charges, E_{NiO} is directly related to the corrected bias voltage as $V - V_{bi} = \Sigma d_i E_i = (\Sigma d_i/\varepsilon_i)\varepsilon_{NiO}E_{NiO}$, and we can define E_{NiO} in the low bias voltage range as $E_{NiO} = (V - V_{bi})/(\varepsilon_{eff}d)$ in terms of effective dielectric permittivity ε_{eff} and inter-electrode gap d ($=\Sigma d_i$).

The data corresponding to the subthreshold bias voltage range in Figure 4 are re-plotted in Figure 5 to show the current density divided by the corrected bias voltage in a log scale as a function of the corrected bias voltage in accordance with a rearrangement of eq 1:

$$\ln[J/(V - V_{bi})] = m(T)\sqrt{V - V_{bi}} + b(T) \quad (2)$$

where temperature-dependent slope $m(T)$ and intercept $b(T)$ are

$$m(T) = \frac{q}{kT}\sqrt{\frac{q}{\pi\varepsilon_0\varepsilon_{NiO}\varepsilon_{eff}d}} \quad (3)$$

and

$$b(T) = -\frac{q\varphi_t^{NiO}}{kT} + \ln C' = -\frac{q\varphi_t^{NiO}}{kT} + \ln\frac{C}{\varepsilon_{eff}d} \quad (4)$$

A linear variation of $\ln[J/(V - V_{bi})]$ with respect to $(V - V_{bi})^{1/2}$ indicates that the PF emission mechanism is indeed responsible for the hole-only currents.

The values of $m(T)$ and $b(T)$ corresponding to best-fit lines in Figure 5 are determined from linear regression analyses and plotted in Figure 6. Both $m(T)$ and $b(T)$ are inversely proportional to T as expected from eqs 3 and 4. The values of

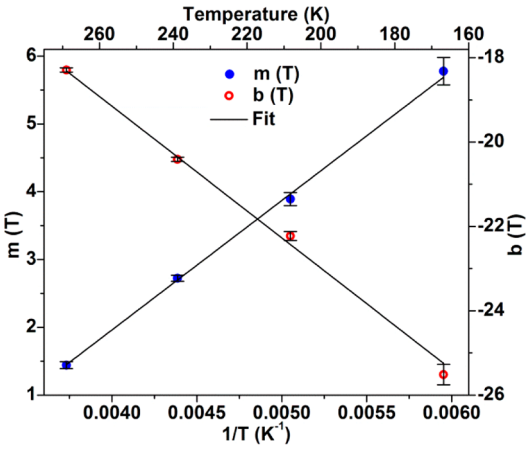

Figure 6. Variations of the temperature-dependent coefficients $m(T)$ and $b(T)$, the values of which were extracted from the best-fit lines in Figure 5, with respect to $1/T$.

dx.doi.org/10.1021/am500593a | ACS Appl. Mater. Interfaces 2014, 6, 7286–7291

ε_{NiO} and ϕ_t^{NiO} are determined from a detailed analysis of $1/T$-dependent variations of $m(T)$ and $b(T)$. If we assume that the relative dielectric permittivity is 3.5 for both organic layers (Poly-TPD and Alq_3)[26−28] and 8 for a QD layer,[29,30] then that of a NiO layer is deduced as 3.0 ± 0.1. Concomitantly, the value of ϕ_t^{NiO} is determined as 0.27 ± 0.01 eV. The relative dielectric permittivity of 3.0 ± 0.1 is consistent with that of sol−gel NiO films in a previous report.[31] The emission barrier height of 0.27 ± 0.01 eV is larger than the previously reported value of 0.2 eV for MOCVD-grown epitaxial NiO films on AlGaN/GaN heterostructures.[10] We attribute the discrepancy in emission barrier heights to the difference in crystal quality and morphology between NiO films. As a typical atomic force microscopy (AFM) image in the inset of Figure 2 shows, sol−gel NiO films had a granular morphology in contrast to epitaxial MOCVD films. Nevertheless, a root-mean-square (RMS) roughness estimated from the AFM image is only 0.63 nm, and therefore, devices with a neat and compact QD EML can be fabricated with a sol−gel NiO HIL.

Beyond the threshold voltage for luminance turn-on, both hole and electron flows contribute to the measured currents. Hence, it is not straightforward to quantitatively elucidate current variations with respect to applied bias voltages without a rigorous full-scale simulation. However, the current−density variations show a distinctive dependence on the corrected bias voltage, which is given as[22]

$$J = \alpha(T)(V - V_{bi})^2 \exp[0.89\beta(T)\sqrt{V - V_{bi}}] \quad (5)$$

where α(T) is an overall proportional coefficient and β(T) is a coefficient that determines the electric field dependence of the mobility. We note that eq 5 resembles a SCLC model modified with a PF-type mobility that depends on temperature and electric field.[22] Such a mobility is consistent with charge transport by hopping between adjacent localized states induced by disorder.[32]

Plots of $\ln[J/(V - V_{bi})^2]$ with respect to $(V - V_{bi})^{1/2}$ in Figure 7 show a linear variation in accordance with eq 5. It is interesting to note that α and β, the values of which correspond to the best-fit lines determined from linear regression analyses, have contradistinctive temperature dependence. As functions of $1/T$, α decreases exponentially, and β increases linearly. Both the Arrhenius-like behavior of α and the linear $1/T$-dependence of β are consistent with the PF-type mobility that represents thermally-activated hopping transport of charge carriers.[33] Among many factors lumped into α(T), only a zero-field mobility has the Arrhenius-like behavior with an energy barrier for hopping. Therefore, the magnitude of hopping barrier Δ can be deduced by fitting α(T) to the functional form of $\alpha_0 \exp(-\Delta/kT)$ with a constant α_0. The activation energy corresponding to the Arrhenius plot in the inset of Figure 7 is 0.11 ± 0.01 eV.

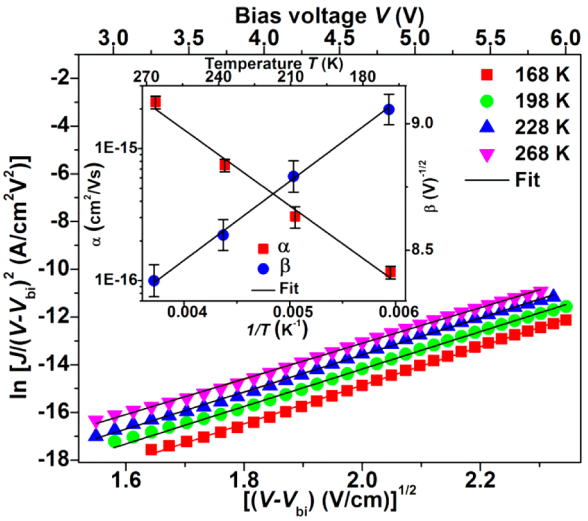

Figure 7. In accordance with the SCLC model modified with a PF-type mobility, the J−V curves of the NiO device (see Figure 3) in a high bias voltage range above the threshold for luminance turn-on are redrawn in the form of $\ln J/(V - V_{bi})$ versus $(V - V_{bi})^{1/2}$ at different temperatures. Inset shows the Arrhenius plot of deduced α(T) values together with a best-fit line.

CONCLUSION

We have demonstrated that the charge transport in the QLED device based on colloidal CdSe/ZnS QDs and having a NiO HIL can be elucidated by taking into account localized trap states which are bound to occur in sol−gel NiO films with a granular morphology. In particular, the PF emission mechanism referring to electric-field-enhanced thermal emission of charge carriers from Coulombic traps and the SCLC model modified with the PF-type mobility to account for the charge transport by hopping between adjacent localized states rule the current−density variations with respect to $(V - V_{bi})^{1/2}$ in bias voltage ranges below and above the luminance turn-on threshold, respectively. The suppression of excessive hole currents in the NiO device, which led to a substantial luminous-efficiency increase compared to the PEDOT:PSS device, was the most important contribution of the sol−gel NiO HIL. Other measures of efficiency were improved as well, and additionally, light emission with high color purity occurred from the NiO device. The use of sol−gel NiO films is important because it can be a good platform for easy implementation of photonic structures by using techniques such as contact printing.

EXPERIMENTAL SECTION

QLED devices having a multilayer structure of ITO/NiO/Poly-TPD/QD/Alq_3/LiF/Al were fabricated and characterized. An ITO layer having 22 Ω/sq. sheet resistance is a transparent conducting anode, a 20 nm NiO layer is a HIL, a 20 nm poly-TPD layer is a HTL, a 20 nm QD layer is an EML, a 40 nm Alq_3 layer is an electron transport layer (ETL), and a combination of LiF/Al is a cathode. For comparison, control devices were fabricated by replacing the NiO HIL with a PEDOT:PSS layer.

Device fabrication, the details of which were previously reported,[23] is only briefly described here. First, a piece of ITO glass was thoroughly cleaned, and the ITO layer was patterned into an anode. Second, a patterned ITO anode was plasma treatment prior to spin-coating a precursor for a sol−gel NiO layer, which was a diethanolamine-added solution of nickel acetate tetrahydrate in methanol. Third, we carried out thermal annealing in a tube furnace at 425 °C for 10 min to transform the precursor coating into a dense film of polycrystalline NiO.[5] Next, a poly-TPD HTL was spin-coated from a chlorobenzene solution, and a QD EML was spin-coated from a solution of colloidal CdSe/ZnS QDs in toluene. Both a poly-TPD HTL and a QD EML were spin-coated in a glovebox. Finally, an Alq_3 ETL and a LiF/Al cathode were deposited by thermal evaporation at the vacuum of 3×10^{-6} Torr. The growth rates for Alq_3 and Al were 1 Å/s and that for LiF was 0.1 Å/s. The area of a square pixel defined by the anode−cathode overlap was 3×3 mm^2. All fabricated devices were hermetically sealed by glass encapsulation with enclosed getter.

A Keithley 236 source-measurement unit was used to measure currents with respect to bias voltages, and a Minolta CS-100A was

dx.doi.org/10.1021/am500593a | ACS Appl. Mater. Interfaces 2014, 6, 7286−7291

used for concomitant luminance measurement. Electroluminescence (EL) and photoluminescence (PL) spectra were measured by using a Darsa Pro-5000 System and an F-7000 spectrofluorometer, respectively. The conduction mechanism of NiO layers in a QLED device was investigated by comparing the temperature dependence of $J-V$ characteristics measured in high vacuum ($\sim 10^{-7}$ Torr) at temperatures of 168, 198, 228, and 268 K.

■ ASSOCIATED CONTENT

Supporting Information

Tables S1 and S2: the values and corresponding uncertainties of parameters m, b, α, and β, which we deduced from their temperature dependence. Figure S1: a typical surface profile that shows surface roughness of sol−gel NiO layers with a granular morphology and the corresponding original AFM image enlarged. This material is available free of charge via the Internet at http://pubs.acs.org.

■ AUTHOR INFORMATION

Corresponding Author

*E-mail: soonil@ajou.ac.kr.

Present Address

[§]H.T.N.: Department of Nanophotonics Technology, Faculty of Engineering Physics and Nanonotechnology, University of Engineering and Technology, VNU, Hanoi, Vietnam.

Notes

The authors declare no competing financial interest.

■ ACKNOWLEDGMENTS

This work was supported by the National Research Foundation of Korea through the Priority Research Centers Program (NRF-2009-0094046) and by Ajou University through the Excellence Research Program in 2010.

■ REFERENCES

(1) Chan, I.-M.; Hsu, T.-Y.; Hong, F. C. Enhanced Hole Injections in Organic Light-Emitting Devices by Depositing Nickel Oxide on Indium Tin Oxide Anode. *Appl. Phys. Lett.* **2002**, *81*, 1899−1901.

(2) Chan, I.-M.; Hong, F. C. Improved Performance of the Single-Layer and Double-Layer Organic Light Emitting Diodes by Nickel Oxide Coated Indium Tin Oxide Anode. *Thin Solid Films* **2004**, *450*, 304−311.

(3) Im, H. C.; Choo, D. C.; Kim, T. W.; Kim, J. H.; Seo, J. H.; Kim, Y. K. Highly Efficient Organic Light-Emitting Diodes Fabricated Utilizing Nickel-Oxide Buffer Layers between the Anodes and the Hole Transport Layers. *Thin Solid Films* **2007**, *515*, 5099−5102.

(4) Caruge, J.-M.; Halpert, J. E.; Bulovic, V.; Bawendi, M. G. NiO as an Inorganic Hole-Transporting Layer in Quantum-Dot Light-Emitting Devices. *Nano Lett.* **2006**, *6*, 2991−2994.

(5) Ho, J.-K.; Jong, C.-S.; Chiu, C. C.; Huang, C.-N.; Shih, K.-K.; Chen, L.-C.; Chen, F.-R.; Kai, J.-J. Low-Resistance Ohmic Contacts to P-Type GaN Achieved by the Oxidation of Ni/Au Films. *J. Appl. Phys.* **1999**, *86*, 4491−4497.

(6) Chen, H.-L.; Lu, Y.-M.; Hwang, W.-S. Characterization of Sputtered NiO Thin Films. *Surf. Coat. Technol.* **2005**, *198*, 138−142.

(7) Kaneko, N.; Machida, O.; Yanagihara, M.; Iwakami, S.; Baba, R.; Goto, H.; Iwabuchi, A. Normally-off AlGaN/GaN HFETs Using NiO X Gate with Recess. *Power Semiconductor Devices and ICs (ISPSD 2009). 21st International Symposium*, 14−18 June 2009, Barcelona, Spain; pp 2528.

(8) Roccaforte, F.; Greco, G.; Fiorenza, P.; Raineri, V.; Malandrino, G.; Nigro, R. L. Epitaxial NiO Gate Dielectric on AlGaN/GaN Heterostructures. *Appl. Phys. Lett.* **2012**, *100*, 063511.

(9) Roccaforte, F.; Iucolano, F.; Giannazzo, F.; Alberti, A.; Raineri, V. Nanoscale Carrier Transport in Ti/Al/Ni/Au Ohmic Contacts on AlGaN Epilayers Grown on Si (111). *Appl. Phys. Lett.* **2006**, *89*, 022103.

(10) Fiorenza, P.; Greco, G.; Giannazzo, F.; Nigro, R. L.; Roccaforte, F. Poole-Frenkel Emission in Epitaxial Nickel Oxide on AlGaN/GaN Heterostructures. *Appl. Phys. Lett.* **2012**, *101*, 172901.

(11) Mashford, B. S.; Nguyen, T.-L.; Wilson, G. J.; Mulvaney, P. All-Inorganic Quantum-Dot Light-Emitting Devices Formed via Low-Cost, Wet-Chemical Processing. *J. Mater. Chem.* **2010**, *20*, 167−172.

(12) Coe, S.; Woo, W.-K.; Bawendi, M.; Bulović, V. Electroluminescence from Single Monolayers of Nanocrystals in Molecular Organic Devices. *Nature* **2002**, *420*, 800−803.

(13) Coe-Sullivan, S.; Woo, W.-K.; Steckel, J. S.; Bawendi, M.; Bulović, V. Tuning the Performance of Hybrid Organic/Inorganic Quantum Dot Light-Emitting Devices. *Org. Electron.* **2003**, *4*, 123−130.

(14) Coe-Sullivan, S.; Steckel, J. S.; Woo, W.-K.; Bawendi, M. G.; Bulović, V. Large-Area Ordered Quantum-Dot Monolayers via Phase Separation During Spin-Casting. *Adv. Funct. Mater.* **2005**, *15*, 1117−1124.

(15) Sun, Q.; Wang, Y. A.; Li, L. S.; Wang, D.; Zhu, T.; Xu, J.; Yang, C.; Li, Y. Bright, Multicoloured Light-Emitting Diodes Based on Quantum Dots. *Nat. Photonics* **2007**, *1*, 717−722.

(16) Ho, M. D.; Kim, D.; Kim, N.; Cho, S. M.; Chae, H. Polymer and Small Molecule Mixture for Organic Hole Transport Layers in Quantum Dot Light-Emitting Diodes. *ACS Appl. Mater. Interfaces* **2013**, *5*, 12369−12374.

(17) Yang, X.; Ma, Y.; Mutlugun, E.; Zhao, Y.; Leck, K. S.; Tan, S. T.; Demir, H. V.; Zhang, Q.; Du, H.; Sun, X. W.; et al. Stable, Efficient, and All Solution-Processed Quantum Dot Light-Emitting Diodes with Double-Sided Metal-Oxide Nanoparticle Charge Transport Layers. *ACS Appl. Mater. Interfaces* **2014**, *6*, 495−499.

(18) Mueller, A. H.; Petruska, M. A.; Achermann, M.; Werder, D. J.; Akhadov, E. A.; Koleske, D. D.; Hoffbauer, M. A.; Klimov, V. I. Multicolor Light-Emitting Diodes Based on Semiconductor Nanocrystals Encapsulated in GaN Charge Injection Layers. *Nano Lett.* **2005**, *5*, 1039−1044.

(19) Tuan, N. H.; Koh, K. H.; Nga, P. T.; Lee, S. Effect of Cathodes on High Efficiency Inorganic−Organic Hybrid LEDs Based on CdSe/ZnS Quantum Dots. *J. Cryst. Growth* **2011**, *326*, 109−112.

(20) Fiorenza, P.; Lo Nigro, R.; Raineri, V.; Lombardo, S.; Toro, R. G.; Malandrino, G.; Fragalà, I. L. From Micro-to Nanotransport Properties in Pr 2 O 3-Based Thin Layers. *J. Appl. Phys.* **2005**, *98*, 044312.

(21) Zhang, H.; Miller, E. J.; Yu, E. T. Analysis of Leakage Current Mechanisms in Schottky Contacts to GaN and $Al_{0.25}Ga_{0.75}N$/GaN Grown by Molecular-Beam Epitaxy. *J. Appl. Phys.* **2006**, *99*, 023703.

(22) Murgatroyd, P. N. Theory of Space-Charge-Limited Current Enhanced by Frenkel Effect. *J. Phys. D: Appl. Phys.* **1970**, *3*, 151−156.

(23) Nguyen, H. T.; Nguyen, N. D.; Lee, S. Application of Solution-Processed Metal Oxide Layers as Charge Transport Layers for CdSe/ZnS Quantum-Dot LEDs. *Nanotechnology* **2013**, *24*, 115201.

(24) Malliaras, G. G.; Salem, J. R.; Brock, P. J.; Scott, C. Electrical Characteristics and Efficiency of Single-Layer Organic Light-Emitting Diodes. *Phys. Rev. B* **1998**, *58*, R13411−R13414.

(25) Jeglinski, S. A.; Amir, O.; Wei, X.; Vardeny, Z. V.; Shinar, J.; Cerkvenik, T.; Chen, W.; Barton, T. J. Symmetric Light Emitting Devices from Poly (p-Di Ethynylene Phenylene)(p-Di Phenylene Vinylene) Derivatives. *Appl. Phys. Lett.* **1995**, *67*, 3960−3962.

(26) Park, H.; Shin, D.-S.; Yu, H.-S.; Chae, H.-B. Electron Mobility in Tris (8-Hydroxyquinoline) Aluminum (Alq 3) Films by Transient Electroluminescence from Single Layer Organic Light Emitting Diodes. *Appl. Phys. Lett.* **2007**, *90*, 202103.

(27) Nowy, S.; Ren, W.; Wagner, J.; Weber, J. A.; Brütting, W. Impedance Spectroscopy of Organic Hetero-Layer OLEDs as a Probe for Charge Carrier Injection and Device Degradation. *Proc. SPIE 7415, Organic Light Emitting Materials and Devices XIII*, San Diego, CA, 2009; Vol. *7415*, pp 74150G-1−74150G-12.

(28) Brütting, W.; Berleb, S.; Mückl, A. G. Device Physics of Organic Light-Emitting Diodes Based on Molecular Materials. *Org. Electron.* **2001**, *2*, 1−36.
(29) Hummon, M. R.; Stollenwerk, A. J.; Narayanamurti, V.; Anikeeva, P. O.; Panzer, M. J.; Wood, V.; Bulovic, V. Measuring Charge Trap Occupation and Energy Level in CdSe/ZnS Quantum Dots Using a Scanning Tunneling Microscope. *Phys. Rev. B* **2010**, *81*, 115439.
(30) Kannan, V.; Rhee, J. K. Robust Switching Characteristics of CdSe/ZnS Quantum Dot Non-Volatile Memory Devices. *Phys. Chem. Chem. Phys.* **2013**, *15*, 12762−12766.
(31) Aydin, H.; Mansour, S. A.; Aydin, C.; Al-Ghamdi, A. A.; Al-Hartomy, O. A.; El-Tantawy, F.; Yakuphanoglu, F. Optical Properties of Nanostructure Boron Doped NiO Thin Films. *J. Sol-Gel Sci. Technol.* **2012**, *64*, 728−733.
(32) Gonzalez-Vazquez, J. P.; Anta, J. A.; Bisquert, J. Random Walk Numerical Simulation for Hopping Transport at Finite Carrier Concentrations: Diffusion Coefficient and Transport Energy Concept. *Phys. Chem. Chem. Phys.* **2009**, *11*, 10359−10367.
(33) Coropceanu, V.; Cornil, J.; da Silva Filho, D. A.; Olivier, Y.; Silbey, R.; Brédas, J.-L. Charge Transport in Organic Semiconductors. *Chem. Rev.* **2007**, *107*, 926−952.